

Binary Chalcogenides and Their Photocatalytic Water-Splitting Activities

Subjects: Materials Science, Characterization & Testing

Contributor: Mohammad Mansoob Khan, Ashmalina Rahman

Chalcogenides are essential in the conversion of solar energy into hydrogen fuel due to their narrow band gap energy. H₂ is a clean fuel, and its usage can address many of the issues caused by using fossil fuels. It is widely used as a feedstock in the chemical industry to produce ammonia, methanol, and various fuels like diesel, gasoline, etc. It is also used as a transport fuel. It has several other applications in the production of metals and agricultural industries. A cost-effective and long-lasting chalcogenide-based photocatalysts can make the H₂ generating process more economical and suitable. The use of binary chalcogenides and their modifications (compounds consisting of only one chalcogen and one electropositive atom) for photocatalytic water splitting will be discussed in the following subsections.

Keywords: chalcogenides ; photocatalysts ; photocatalysis ; semiconductors ; water splitting

1. Cd-Based Chalcogenides

CdS and CdSe have both been used extensively in the fields of photocatalysis and photovoltaics, particularly in photoelectrochemical cells. Despite having a favorable bandgap for water splitting (~2.42 eV) ^{[1][2]} CdS is unstable in an aqueous solution under light irradiation due to photocorrosion. Therefore, in order to improve its photostability and photocatalytic activity, many studies have focused on synthesizing different morphologies of CdS together with the addition of co-catalysts and sacrificial agents ^[2]. Some of the different morphologies of CdS nanostructures that have been studied include hollow spheres ^[3], quasi-nanospheres ^[4], nanowires ^[4], and nanotubes ^[4], all of which can be synthesized by hydrothermal methods. Among these, CdS nanospheres were found to exhibit the highest H₂ evolution rate during photocatalytic testing in the presence of Na₂SO₃ and Na₂S hole scavengers.

In a recent study, one-dimensional CdS nanotubes displayed a remarkably high valence band edge compared with bulk CdS due to quantum confinement effects, and it was found that the photocatalytic efficiency of CdS nanotubes is higher than that of bulk CdS. Furthermore, the stabilized valence band, tubular structure, and strong p-d orbital hybridization led to a significant enhancement in photostability, making applications in aqueous solutions feasible ^[5].

In addition to the aforementioned studies focused on enhancing CdS through the preparation of different morphologies and sizes, another strategy to impart anti-photocorrosion properties to CdS is surface-modification with non-noble co-catalysts such as Ni, Ni₂P, and CuS-Ni_xP ^{[6][7][8]} as well as noble metals such as Pt and Au ^{[9][10]}.

Another strategy to improve the photostability of CdS in an aqueous solution is to coat it with a thin layer of ZnO. Tso and co-workers have synthesized composite nanowires comprising CdS cores covered with thin ZnO shells, yielding CdS/ZnO core-shell nanowires ^[11]. These heterostructures provided improved stability compared with bare CdS nanowires and also led to reduced electron-hole recombination, causing an increase in H₂ evolution activity of over two orders of magnitude as shown in **Figure 1**. Investigations also revealed that nanowires with 10–30 nm-thick shells absorbed more incident light than nanowires with thinner ZnO shells and had a lower probability of electron-hole recombination, the combination of which led to higher H₂ evolution activity.

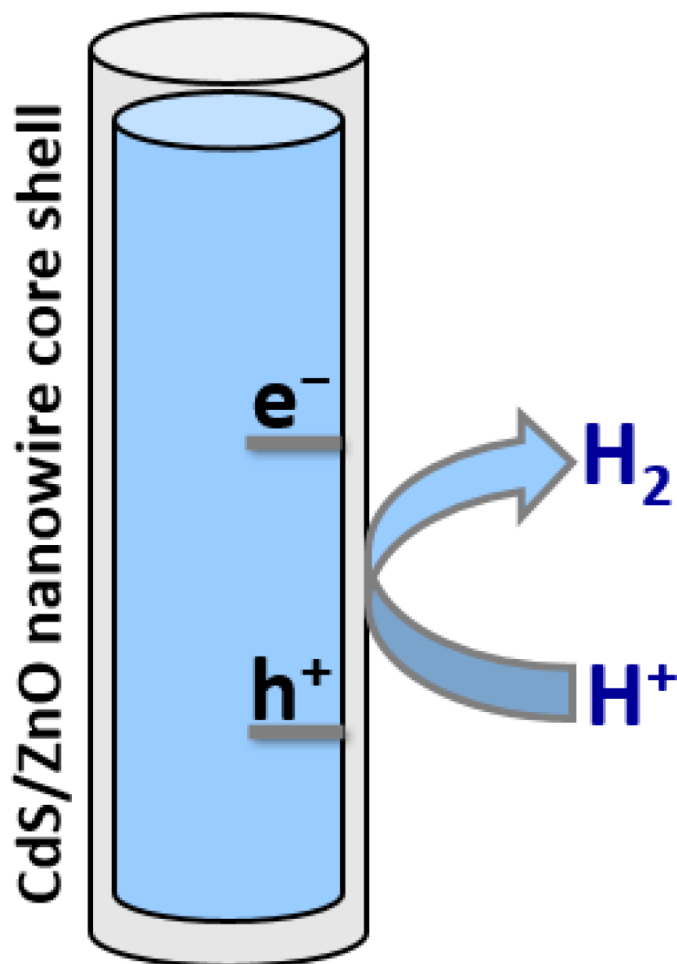


Figure 1. Schematic diagram of photocatalytic H₂ production using CdS/ZnO core-shell nanowire.

Several recent studies have examined photogenerated electron-hole pair separation in CdS/CuS nanocomposites [11]. Pan and co-workers found a high H₂ evolution rate of 561.7 $\mu\text{mol h}^{-1}$ during photocatalytic water splitting using a CdS/CuS nanocomposite [12]. In another work, a CdS/CuS nanostructured heterojunction was synthesized [13]. The prepared material was applied as a water-splitting photocatalyst and showed that the nanocomposites exhibit an enhanced rate of photocatalytic H₂ evolution under visible-light irradiation. It can be concluded that CuS as a non-noble catalyst can improve the stability of CdS for photocatalytic H₂ production in an aqueous solution. The enhancement in stability found in the CdS/CuS system can be explained by the transfer of holes from CdS to CuS, which inhibits the photocorrosion of CdS (Figure 2) [14].

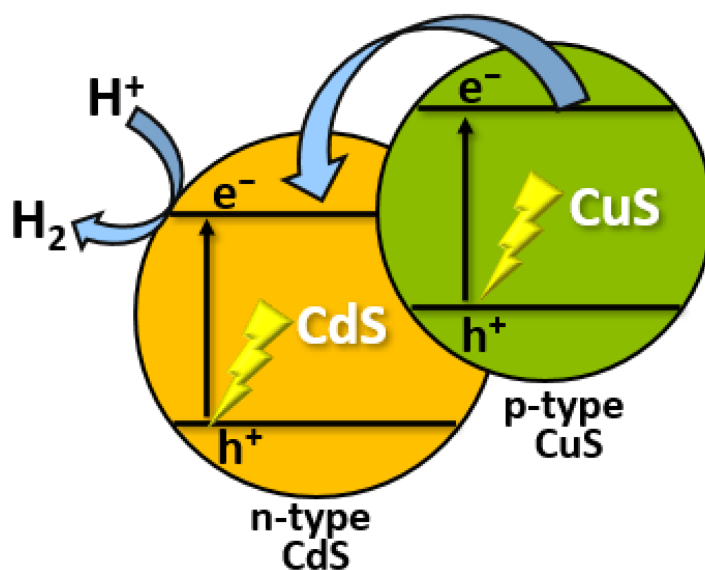


Figure 2. Mechanism of photocatalytic H₂ evolution using CdS/CuS nanocomposite.

Several authors have studied the factors affecting the performance of nanocrystalline CdSe quantum dots (QD) in photocatalytic water-splitting applications. Osterloh and co-workers showed a clear relationship between the extent of

quantum size confinement and the photocatalytic water-splitting activity of suspended CdSe QDs. They found that the rate of H₂ evolution increased with QD size in nm as follows: 2.20 > 2.00 > 2.48 > 1.75 > 2.90 > 2.61 > 2.75 > 3.05 > 3.49 > 4.03 > 4.81. These results confirm that photocatalytic activity can be controlled by the extent of quantum confinement (Figure 3) [15].

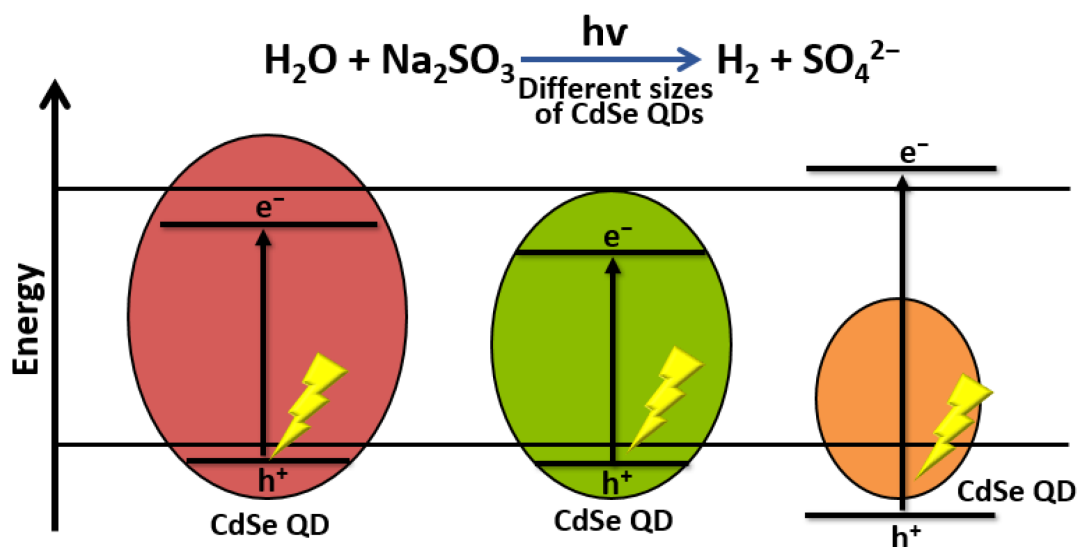


Figure 3. Schematic illustration of the effect of CdSe QD size in photocatalytic H₂ production.

Covalent organic frameworks (COFs) have drawn research interest owing to their stability, porous structure, large surface area, and tunable band structure [16]. It is an organic polymer arranged periodically with high crystallinity and high porosity, that is built from the integration of selected organic blocks via covalent bond linkage [17]. For instance, You et al. have synthesized COFs-p-phenylenediamine@CdS (COFs-Ph@CdS) using the hydrothermal method [18]. The authors reported that of the H₂ generation of bare CdS, COFs-Ph@CdS-x (x = 1, 2, 3, 4) photocatalysts were 16.4, 139.1, 17.5, 37.0, and 15.2 μmol, respectively. The photocatalytic H₂ production activity of solid COFs-Ph@CdS-1 exhibited 29 and eight times higher compared to those of pristine COFs and CdS, respectively. The enhanced activity may be attributed to a stable coordination bond between Cd²⁺ ions and N atoms in COFs-Ph@CdS was formed, which served as a migrated channel for photo-generated carriers and their unique hollow structure that enables the production of more photo-generated electrons and holes and absorb light more efficiently.

High rates of photocatalytic H₂ production were demonstrated by Das and co-workers using a surface ligand that binds strongly to CdSe QDs via tridentate coordination [19]. These authors also reported the effects of surface stabilizing and solubilizing agent dynamics. In more recent work, the influence of ligand exchange on the photocatalytic activity of CdSe QDs in solar water-splitting cells was studied [20]. It was found that CdSe QDs bearing shorter ligands showed better photocatalytic activity when compared to pristine CdSe QDs in a photoelectrochemical cell. These results should assist with the design and optimization of photochemical energy conversion systems employing nanocrystalline CdSe QD photocatalysts.

2. Cu-Based Chalcogenides

Visible-light-active CuS/Au nanostructures were obtained by decorating CuS particles with Au nanoparticles, which were prepared by reducing HAuCl₄ on the CuS surface [21]. The as-synthesized nanostructures displayed excellent catalytic performance in electrochemical H₂ evolution tests, with good durability under acidic conditions. It was found that the CuS/Au nanostructured catalyst could produce a current density of 10 mA/cm² upon the application of only 0.179 V versus the reversible hydrogen electrode (RHE). The CuS/Au catalyst also proved to be an efficient photocatalyst for the degradation of organic pollutants under visible-light irradiation.

The coupling of CuS with metal oxide has been shown to enhance its photocatalytic activities. For instance, Chandra and co-workers have synthesized CuS/TiO₂ heterostructures with varying TiO₂ contents using a simple hydrothermal method for the photocatalytic evolution of H₂ [22]. The highest rate of visible-light photocatalytic H₂ production was 1262 μmol h⁻¹ g⁻¹, which is around 9.7 and 9.3 times faster in comparison to pristine TiO₂ nanospindles or CuS nanoflakes, respectively. The enhanced rate of H₂ evolution is attributable to increased light harvesting and more efficient charge separation when an optimum amount of CuS is deposited on TiO₂. Growing CuS nanoflakes on TiO₂ nanoparticles to form a CuS/TiO₂ heterostructure facilitates charge carrier separation at the heterostructure interface and thus enhances photocatalytic performance.

In another study, Dubale et al. fabricated nanocomposites comprising CuS and Cu₂O/CuO heterostructures with and without decoration by Pt nanoparticles using an in-situ growth method [23]. Cu₂O/CuO was prepared by straightforward anodization of Cu film, and a sputtering technique was used to deposit Pt nanoparticles onto the prepared Cu₂O/CuO/CuS photocathodes. The prepared heterostructures were found to be very promising and highly stable photocathodes for H₂ evolution under visible-light irradiation, with optimized Cu₂O/CuO/CuS photocathodes reaching photocurrent densities of up to 5.4 mA cm⁻², some 2.5 times higher than that achieved by bare Cu₂O/CuO. Upon decorating the Cu₂O/CuO with both CuS and Pt, a further increase in photocurrent density to 5.7 mA/cm² was achieved due to the suppression of the charge carrier recombination.

Metal loading on the surface of Cu-based chalcogenides has been reported to improve the photocatalytic evolution of H₂. For instance, Ma and co-workers have reported that hydrothermally synthesized Au/CuSe/Pt nanoplates showed strong dual-plasmonic resonance and have been employed for photocatalytic H₂ generation under irradiation of visible and near-infrared [24]. The as-prepared Au/CuSe/Pt nanoplates exhibited outstanding H₂ generation activities of around 7.8 and 9.7 times those of Au/CuSe and Pt/CuSe composites, respectively. In the Au/CuSe/Pt system, light harvesting is enhanced by the plasmonic units (CuSe and Au), while Pt is mainly present as a co-catalyst promoting the H₂ evolution reaction as shown in Figure 4.

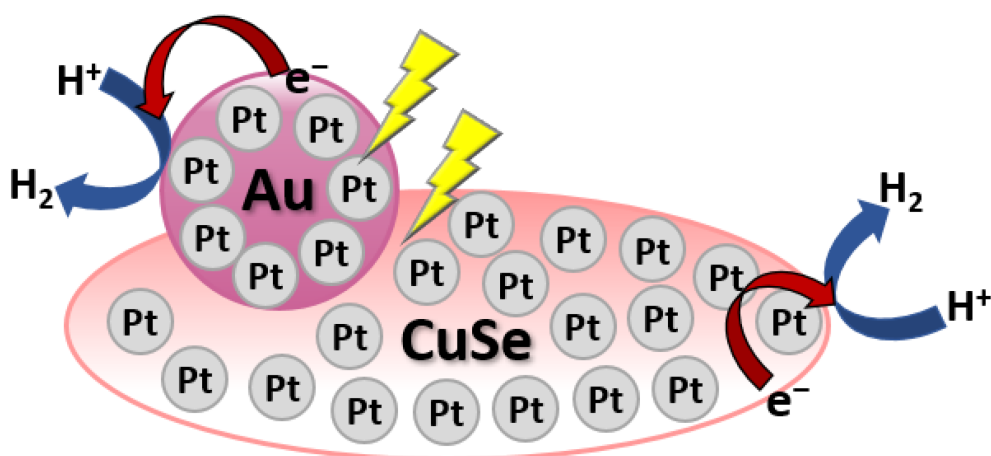


Figure 4. Schematic diagram of Au/CuSe/Pt ultrathin nanoplate hybrid for H₂ evolution under visible and near-infrared irradiation.

3. Ga-Based Chalcogenides

Monolayers of GaS and GaSe have been studied as photocatalysts by several authors but their performance is limited by low optical absorption and inefficient electron-hole pair separation [25][26]. One strategy to overcome these limitations is the construction of van der Waals (vdW) heterostructures by pairing GaX (GaX, X = S, Se) with arsenene (two-dimensional arsenic), as demonstrated by Peng and co-workers using first-principle calculations [27]. Such GaX/As heterostructures possess band gaps and band alignment that satisfy the requirements for photocatalytic water splitting. In contrast to pristine GaX monolayers, the type of band gap in Se_{0.5}GaS_{0.5}/As and S_{0.5}GaSe_{0.5}/As changes favorably from indirect to direct as the interlayer distance is varied. Furthermore, these heterostructures exhibit transport anisotropy with high electron mobilities of up to ~2000 cm² V⁻¹ s⁻¹, which facilitates photogenerated electron-hole pair separation and migration. All of the GaX/As heterostructures studied also show enhanced visible-light absorption beyond that of pristine GaX monolayers. It seems likely that the exceptional properties of GaX/As heterostructures will render them competitive with existing photocatalysts for solar-driven water splitting [27].

4. Mo-Based Chalcogenides

Molybdenum disulfide (MoS₂) is a two-dimensional (2D) material, and it tends to exhibit more remarkable photocatalytic properties than its bulk counterparts [28][29]. Li and co-workers have investigated the photocatalytic properties of pristine MoS₂ nanosheets and Ag-modified MoS₂ nanosheets. They found that the rate of photocatalytic H₂ production by Ag-modified MoS₂ nanosheets could reach 2695 μmol h⁻¹ g⁻¹. They also found that Ag-doped MoS₂ nanosheets exhibit superior stability and higher H₂ evolution efficiency compared with pristine MoS₂ nanosheets, which is mainly due to increased visible-light absorption with increasing Ag content (Figure 5) [30].

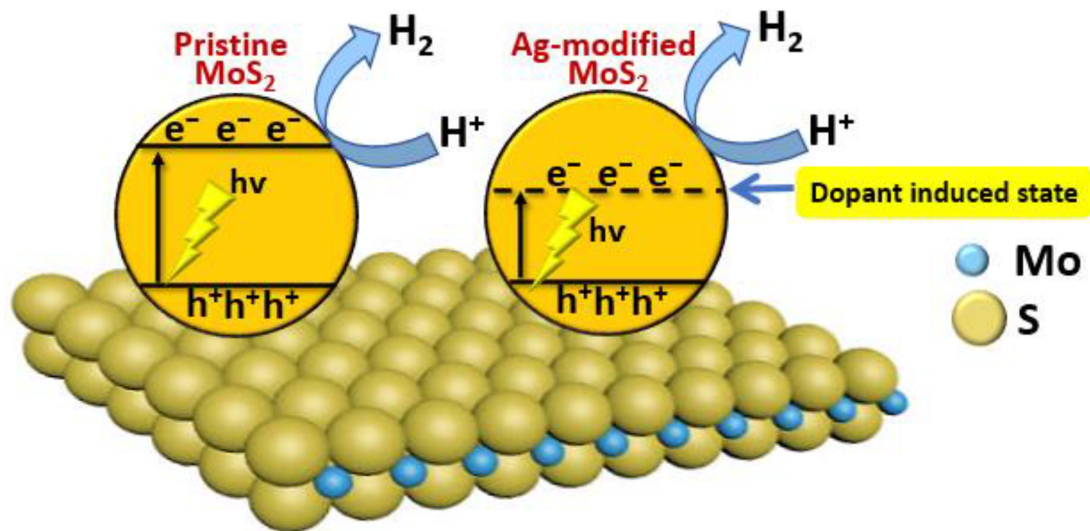


Figure 5. The mechanism of photocatalytic H₂ production using Ag-modified MoS₂ nanosheets.

Photocorrosion-resistant material, MoS₂/Zn_{0.5}Cd_{0.5}S/g-C₃N₄, has been successfully synthesized by Tang et al. to produce H₂ under irradiation of visible light [31]. The authors reported that the as-prepared materials exhibited a maximum H₂ production rate of 4914 μmol g⁻¹h⁻¹ in Na₂S-Na₂SO₃ solutions which served as the sacrificial agent. The high evolution rate of H₂ was owing to the improved charge separation between the interfaces.

In another study, Yuan et al. designed 2D-2D MoS₂@Cu-ZnIn₂S₄ using the solvothermal method for photocatalytic production of H₂ [32]. The highest H₂ evolution rate of 5463 μmol g⁻¹h⁻¹ was observed for 6% MoS₂@Cu-ZnIn₂S₄ under irradiation of visible light which is 72 times higher than that of pristine Cu-ZnIn₂S₄. The excellent activity may be ascribed to the high visible light absorption property and abundant active sites for the H₂ evolution reaction to take place. Moreover, the production rate of H₂ remain unchanged after three cycles which suggested the high durability of the synthesized MoS₂@Cu-ZnIn₂S₄ for photocatalytic H₂ production.

An enhanced photocatalytic H₂ evolution was performed by Yin and co-workers with the maximum evolution rate of 872.3 mol h⁻¹ using MoS₂/C composites sensitized with Erythrosin B [33]. The enhanced performance was attributed to the efficient photo-generated charge transfer and separation between Erythrosin B and MoS₂ or C as well as the presence of more active sites for H₂ evolution. The photocatalytic evolution of H₂ could also be achieved through photoelectrochemical catalytic activities. For instance, Hassan and co-workers have reported the optimized MoS₂/GaN₂ exhibited significantly higher photoelectrochemical performance in comparison to the bare materials under the same visible conditions [34]. The as-prepared photoanode achieved efficient light harvesting with a photocurrent density of 5.2 mA cm⁻² which is 2.6 times higher than bare GaN. Moreover, MoS₂/GaN₂ exhibited enhanced applied-bias-photon-to-current conversion efficiency of 0.91%, while the reference GaN yielded an efficiency of 0.32%. The authors reported that the decrease in charge transfer resistance between the electrolyte and semiconductor interface and the improved separation charge carriers in the MoS₂/GaN heterostructures were all attributed to significant improvements in photocurrent density and efficiency.

MoS₂-based nanomaterials have been found to be an efficient visible light-responsive material for H₂ production. Based on the reported work, revealed that the surface modification of the MoS₂ could lead to an improved photocatalytic activity owing to the effective charge transfer and separation of photo-generated e⁻/h⁺ pairs.

New strategies have been developed to use MoSe₂-based nanosheets as photocatalysts for the H₂ evolution reaction. Zhao and co-workers achieved an enhancement in the photocatalytic activity of MoSe₂ by surface modification and doping with Ni and Co [35]. Their study found that Ni_{0.15}Mo_{0.85}Se₂ nanosheets exhibited the highest photocatalytic activity in both alkaline and acidic media. These results provide an attractive alternative to Pt-based catalysts.

5. Sn-Based Chalcogenides

Recently, it has been discovered that monolayers of the Sn-based mono- and dichalcogenides SnX and SnX₂ (X = S or Se) are promising candidates for photocatalytic water splitting. These materials exhibit very good visible light absorption, low exciton binding energies, and high carrier mobility. However, in their pure and strain-free state, the valence band edges of Sn-monochalcogenide monolayers are predicted to be too high in energy for effective water oxidation. This issue can potentially be overcome by crystal engineering to induce a moderate tensile strain, which is predicted to lower the valence band edge to a level suitable for water oxidation [36]. Li and co-workers reported that monolayers of both SnX and

SnX_2 are expected to exhibit good optical absorption in the visible region of the solar spectrum, and the predicted sequence of visible light absorption strength is as follows: $\text{SnSe} > \text{SnSe}_2 > \text{SnS} > \text{SnS}_2$. Moreover, SnX and SnX_2 monolayers also have excellent carrier mobility, which results in the fast migration of photogenerated carriers to the surface. Hence, the possibility of rapid redox reactions on the surface of the photocatalyst.

In another study, Lei et al. successfully prepared $\text{SnS/g-C}_3\text{N}_4$ nanosheets using a facile ultrasonic and microwave heating approach, which formed intimate interfacial contact and a suitable energy band structure [37]. The optimized sample displayed enhanced photocatalytic H_2 evolution from H_2O with the aid of Pt as a co-catalyst in comparison to pure $\text{g-C}_3\text{N}_4$. The stability of the photocatalysts was significantly improved after being loaded with MoO_3 particles due to the formation of a Z-scheme heterojunction. Among all as-prepared samples, the 10% $\text{SnS/g-C}_3\text{N}_4$ exhibits the highest photocatalytic rate of $818.93 \text{ mmol h}^{-1}\text{g}^{-1}$ under AM1.5G irradiation, 2.90 times to pure $\text{g-C}_3\text{N}_4$, due to the matched energy band structure between $\text{g-C}_3\text{N}_4$ and SnS , which improves the separation efficiency of photo-generated carriers and hinders the recombination of hole-electron pairs. Additionally, SnS nanosheets have improved the light absorption efficiency of the prepared material and generated more catalytic active sites as well as shortening the carriers' transport path as well.

Liu and co-workers have synthesized flower-like nanostructure SnS_2 with generated sulfur vacancies using a new simple strategy of ion exchange [38]. The morphology of the flower-like structure provides shorter carrier diffusion lengths and more surface-active sites. While, the presence of S vacancies helps introduce defect levels in SnS_2 , which leads to a reduction in work function, eventually improving carrier density and separation efficiency. The well-engineered sample 5% Cu/SnS_{2-x} shows the highest photocatalytic activity with an H_2 yield of 1.37 mmol h^{-1} , which is about six times higher than that of pure SnS_2 .

$\text{SnS}_2/\text{ZnIn}_2\text{S}_4$ composites were successfully fabricated by decorating SnS_2 nanosheets with ZnIn_2S_4 microspheres [39]. Geng and co-workers reported that the $\text{SnS}_2/\text{ZnIn}_2\text{S}_4$ composites showed superior photocatalytic properties for H_2 generation in comparison to pristine ZnIn_2S_4 . Furthermore, a notable impact was observed on the photocatalytic activity of ZnIn_2S_4 when varying the mass ratio of SnS_2 . The 2.5% $\text{SnS}_2/\text{ZnIn}_2\text{S}_4$ in particular exhibited the highest photocatalytic H_2 generation rate of $769 \text{ }\mu\text{mol g}^{-1}\text{h}^{-1}$, which was about 10.5 times the photocatalytic activity of pristine ZnIn_2S_4 . The enhanced photocatalytic activity may be due to the formation of $\text{SnS}_2/\text{ZnIn}_2\text{S}_4$ heterojunction, which enabled highly active charge separation and transfers on the interface of SnS_2 and ZnIn_2S_4 .

6. Ti-Based Chalcogenides

The tri-chalcogenide TiS_3 was found to be an effective photoanode for use in photoelectrochemical cells. Photocatalytic H_2 evolution rates of up to $1.80 \pm 0.05 \text{ }\mu\text{mol min}^{-1}$ were obtained, corresponding to a photoconversion efficiency of $\sim 7\%$ [40]. Furthermore, the ternary compounds $\text{Ti}_x\text{Nb}_{1-x}\text{S}_3$ (Nb-rich) and $\text{Nb}_x\text{Ti}_{1-x}\text{S}_3$ (Ti-rich) were tested as photoanodes and compared with the corresponding binary trisulfides. The binary compounds were polycrystalline with a nanoribbon morphology and adopted the monoclinic TiS_3 (P21/m) and triclinic NbS_3 (P2) crystal structures, respectively. H_2 generation experiments revealed that the Ti-rich phase was a superior photocatalyst compared with the Nb-rich phase, exhibiting H_2 production rates of up to $2.2 \pm 0.1 \text{ mol/min cm}^2$ [41]. Ti-based chalcogenides are not widely explored for their photocatalytic H_2 production activity. Therefore, further studies and optimizations are required.

7. V-Based Chalcogenides

Certain transition metals located on the first row of the periodic table can participate in the formation of tetra-chalcogenides thanks to their ability to adopt +4 oxidation states (Figure 6). Among these metals is vanadium, which can form the binary tetra-chalcogenide VS_4 . Nanocomposites comprising VS_4 and graphene were evaluated for solar-driven water splitting by Guo and co-workers. Excellent performance was obtained due to the formation of C-S bonds with a π -conjugated structure, which assists with transferring electrons from the S 2p orbital to graphene [42]. The ternary tetra-chalcogenides $\text{Cu}_3\text{Nb}_{1-x}\text{V}_x\text{S}_4$ and $\text{Cu}_3\text{Ta}_{1-x}\text{V}_x\text{S}_4$, which exist as solid solutions and adopt the sulvanite structure, were successfully synthesized in a solid-state reaction by Ikeda and co-workers [43]. The band gaps of the synthesized materials were estimated to fall in the range of 1.6–1.7 eV, and the band structure of the $\text{Cu}_3\text{M}_{1-x}\text{V}_x\text{S}_4$ system varies with composition. It was found that for most compositions of solid solution, superior photocatalytic activity was achieved compared with the ternary Cu_3MS_4 (M = V, Nb, Ta) compounds [43].

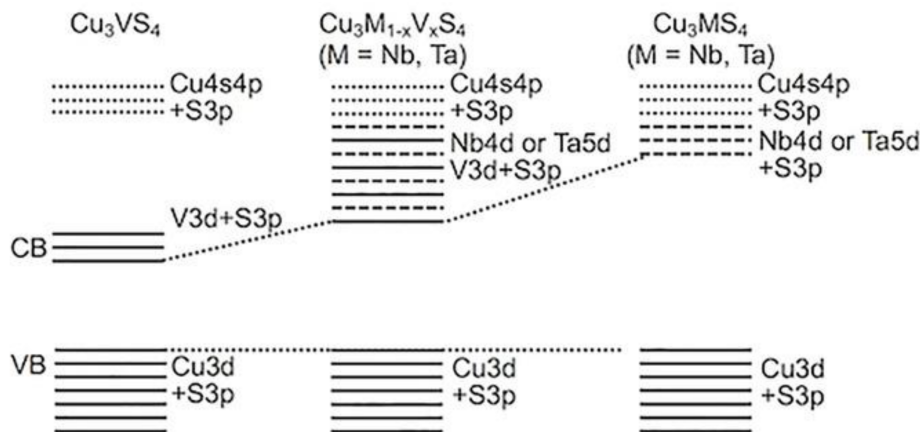


Figure 6. Proposed band structures for $\text{Cu}_3\text{M}_{1-x}\text{V}_x\text{S}_4$ ($\text{M} = \text{Nb}$ and Ta) solid solutions.

Li et al. synthesized the $\text{VS}_2@\text{C}_3\text{N}_4$ heterojunction with S vacancies via the in situ supramolecular self-assembly method [44]. The as-synthesized material shows a remarkable synergistic H_2 production rate ($9628 \mu\text{mol g}^{-1}\text{h}^{-1}$) and wastewater degradation efficiency as well as stability, which is 16.0 times that of pristine C_3N_4 . Based on the theoretical calculations and experiment findings, it shows that S vacancies have resulted in the formation of compact heterostructure and the reduction in the work function, which promotes interfacial carriers' transfer and surface properties. The core-shell structure improves the stability of S vacancies.

In another study, Gopalakrishnan et al. synthesized a core-shell heterostructures photocathode consisting of VS_2 deposited on a silicon nanowire surface via single-step chemical vapor deposition for H_2 evolution under solar irradiation [45]. The core-shell nanowire heterostructure photocathode displayed an outstanding solar-assisted water reduction performance at $\text{pH} \sim 7$ over a pristine photocathode. The as-prepared material produces about $23 \mu\text{mol cm}^{-2} \text{h}^{-1}$ (at 0 V vs. RHE) of H_2 gas. Recently, Zhong et al. have doped Ni_3S_2 with nitrogen and coupled it with VS_2 using the hydrothermal method [46]. Based on their results, $\text{Ni}_3\text{S}_2/\text{VS}_2$ without nitrogen doping exhibited improved oxygen evolution reaction (OER) performance with an extremely low overpotential of 227 mV at 10 mA/cm^2 which may be attributed to the presence of high number of active sites and excellent interfaces. Moreover, $\text{Ni}_3\text{S}_2/\text{VS}_2$ with nitrogen doping shows high electrocatalytic hydrogen evolution reaction (HER) performance with a low HER overpotential (151 mV at 10 mA/cm^2) and this is due to the presence of nitrogen doping that significantly improves the conductivity and increases the number of catalytic active sites.

8. Zn-Based Chalcogenides

Kurnia and co-workers have investigated the performance of ZnS thin films during photoelectrochemical H_2 generation [47]. They found that ZnS is an inexpensive photocatalyst that exhibits activity under visible-light irradiation without the addition of a co-catalyst. The ZnS thin films were estimated to have band gaps of $\sim 2.4 \text{ eV}$, and photocurrent densities exceeding 1.5 mA/cm^2 were achieved under visible-light irradiation ($\lambda \geq 435 \text{ nm}$). These photocurrents are remarkably high for H_2 generation by undoped ZnS under visible-light irradiation.

A modification of ZnO nanosheets, using a thin layer of ZnS, was developed to enhance visible light absorption, leading to improved photoelectrochemical activity in water-splitting experiments [48][49]. Sánchez-Tovar and co-workers have prepared ZnO/ZnS heterostructures using anodization of Zn in glycerol/water/ NH_4F electrolytes under controlled hydrodynamic conditions in the presence of various concentrations of Na_2S [48]. In another work, Zhang et al. synthesized ZnS/ZnO/ZnS sandwich nanosheets with an effective band gap of $\sim 2.72 \text{ eV}$ using thermal evaporation, and these materials resulted in potent visible-light photocatalytic activity [49]. These works show that coating ZnO with an ultrathin surface layer of ZnS is an interesting approach for enhancing its water-splitting activity under solar irradiation.

Arai and co-workers have synthesized hollow Cu-doped ZnS particles as visible-light photocatalysts for the decomposition of hydrogen sulfide under solar irradiation to generate H_2 . The Cu-doped ZnS particles were synthesized starting from a ZnO precursor that was co-precipitated on Cu by exploiting the difference in reduction potential between Zn and Cu. The visible-light photoactivity of Cu-doped ZnS was six- and 130-times higher than the Cu-free "ZnS-shell" and pristine ZnS particles prepared using co-precipitation, respectively. A comparative study found that the "Cu-ZnS-shell" particles were highly active under visible-light irradiation ($\lambda > 440 \text{ nm}$), and the rate of H_2 evolution was optimized with a Cu (2 wt%)/ZnS photocatalyst [50]. In another recent study, Cu/ZnS microspheres were prepared using a template-free microwave

irradiation method for H₂ generation from an aqueous Na₂S solution under visible-light irradiation. The optimized H₂ evolution rate of 973.1 μmol h⁻¹ g⁻¹ was obtained for 2.0 mol% Cu-doped ZnS [51].

References

1. Oliva, A. Formation of the band gap energy on CdS thin films growth by two different techniques. *Thin Solid Films* 2001, 391, 28–35.
2. Cheng, L.; Xiang, Q.; Liao, Y.; Zhang, H. CdS-Based photocatalysts. *Energy Environ. Sci.* 2018, 11, 1362–1391.
3. Wang, X.; Feng, Z.; Fan, D.; Fan, F.; Li, C. Shape-Controlled Synthesis of CdS Nanostructures via a Solvothermal Method. *Cryst. Growth Des.* 2010, 10, 5312–5318.
4. Li, C.; Yuan, J.; Han, B.; Shangguan, W. Synthesis and photochemical performance of morphology-controlled CdS photocatalysts for hydrogen evolution under visible light. *Int. J. Hydrogen Energy* 2011, 36, 4271–4279.
5. Garg, P.; Bhauriyal, P.; Mahata, A.; Rawat, K.S.; Pathak, B. Role of Dimensionality for Photocatalytic Water Splitting: CdS Nanotube versus Bulk Structure. *ChemPhysChem* 2018, 20, 383–391.
6. Luo, M.; Liu, Y.; Hu, J.; Liu, H.; Li, J. One-Pot Synthesis of CdS and Ni-Doped CdS Hollow Spheres with Enhanced Photocatalytic Activity and Durability. *ACS Appl. Mater. Interfaces* 2012, 4, 1813–1821.
7. Zhen, W.; Ning, X.; Yang, B.; Wu, Y.; Li, Z.; Lu, G. The enhancement of CdS photocatalytic activity for water splitting via anti-photocorrosion by coating Ni₂P shell and removing nascent formed oxygen with artificial gill. *Appl. Catal. B Environ.* 2018, 221, 243–257.
8. Li, Y.-H.; Qi, M.-Y.; Li, J.-Y.; Tang, Z.-R.; Xu, Y.-J. Noble metal free hybrid with modulated charge transfer for enhanced photocatalytic performance. *Appl. Catal. B Environ.* 2019, 257, 117934.
9. Yang, J.; Yan, H.; Wang, X.; Wen, F.; Wang, Z.; Fan, D.; Shi, J.; Li, C. Roles of cocatalysts in Pt–PdS/CdS with exceptionally high quantum efficiency for photocatalytic hydrogen production. *J. Catal.* 2012, 290, 151–157.
10. Yang, T.-T.; Chen, W.-T.; Hsu, Y.-J.; Wei, K.-H.; Lin, T.-Y. Interfacial Charge Carrier Dynamics in Core–Shell Au–CdS Nanocrystals. *J. Phys. Chem. C* 2010, 114, 11414–11420.
11. Tso, S.; Li, W.-S.; Wu, B.-H.; Chen, L.-J. Enhanced H₂ production in water splitting with CdS–ZnO core-shell nanowires. *Nano Energy* 2017, 43, 270–277.
12. Zhang, F.; Zhuang, H.-Q.; Zhang, W.; Yin, J.; Cao, F.-H.; Pan, Y.-X. Noble-metal-free CuS/CdS photocatalyst for efficient visible-light-driven photocatalytic H₂ production from water. *Catal. Today* 2018, 330, 203–208.
13. Cheng, F.; Xiang, Q. A solid-state approach to fabricate a CdS/CuS nano-heterojunction with promoted visible-light photocatalytic H₂-evolution activity. *RSC Adv.* 2016, 6, 76269–76272.
14. Wu, Z.; Zhao, G.; Zhang, Y.-N.; Tian, H.; Li, D. Enhanced Photocurrent Responses and Antiphotocorrosion Performance of CdS Hybrid Derived from Triple Heterojunction. *J. Phys. Chem. C* 2012, 116, 12829–12835.
15. Holmes, M.A.; Townsend, T.K.; Osterloh, F.E. Quantum confinement controlled photocatalytic water splitting by suspended CdSe nanocrystals. *Chem. Commun.* 2011, 48, 371–373.
16. Yang, Q.; Luo, M.; Liu, K.; Cao, H.; Yan, H. Covalent organic frameworks for photocatalytic applications. *Appl. Catal. B Environ.* 2020, 276, 119174.
17. You, J.; Zhao, Y.; Wang, L.; Bao, W. Recent developments in the photocatalytic applications of covalent organic frameworks: A review. *J. Clean. Prod.* 2021, 291, 125822.
18. You, D.; Pan, Z.; Cheng, Q. S-scheme heterojunctions with photocatalytic hydrogen evolution and efficient degradation properties. *J. Alloys Compd.* 2023, 930, 167069.
19. Das, A.; Han, Z.; Haghghi, M.G.; Eisenberg, R. Photogeneration of hydrogen from water using CdSe nanocrystals demonstrating the importance of surface exchange. *Proc. Natl. Acad. Sci. USA* 2013, 110, 16716–16723.
20. Park, Y.; Park, B. Effect of ligand exchange on photocurrent enhancement in cadmium selenide (CdSe) quantum dot water splitting cells. *Results Phys.* 2018, 11, 162–165.
21. Basu, M.; Nazir, R.; Fageria, P.; Pande, S. Construction of CuS/Au Heterostructure through a Simple Photoreduction Route for Enhanced Electrochemical Hydrogen Evolution and Photocatalysis. *Sci. Rep.* 2016, 6, 34738.
22. Chandra, M.; Bhunia, K.; Pradhan, D. Controlled Synthesis of CuS/TiO₂ Heterostructured Nanocomposites for Enhanced Photocatalytic Hydrogen Generation through Water Splitting. *Inorg. Chem.* 2018, 57, 4524–4533.

23. Dubale, A.A.; Tamirat, A.G.; Chen, H.-M.; Berhe, T.A.; Pan, C.-J.; Su, W.-N.; Hwang, B.-J. A highly stable CuS and CuS–Pt modified Cu₂O/CuO heterostructure as an efficient photocathode for the hydrogen evolution reaction. *J. Mater. Chem. A* 2015, 4, 2205–2216.
24. Ma, L.; Yang, D.-J.; Song, X.-P.; Li, H.-X.; Ding, S.-J.; Xiong, L.; Qin, P.-L.; Chen, X.-B. Pt Decorated (Au Nanosphere)/(CuSe Ultrathin Nanoplate) Tangential Hybrids for Efficient Photocatalytic Hydrogen Generation via Dual-Plasmon-Induced Strong VIS–NIR Light Absorption and Interfacial Electric Field Coupling. *Sol. RRL* 2019, 4, 1900376.
25. Zhuang, H.L.; Hennig, R.G. Single-Layer Group-III Monochalcogenide Photocatalysts for Water Splitting. *Chem. Mater.* 2013, 25, 3232–3238.
26. Peng, Q.; Xiong, R.; Sa, B.; Zhou, J.; Wen, C.; Wu, B.; Anpo, M.; Sun, Z. Computational mining of photocatalysts for water splitting hydrogen production: Two-dimensional InSe-family monolayers. *Catal. Sci. Technol.* 2017, 7, 2744–2752.
27. Peng, Q.; Guo, Z.; Sa, B.; Zhou, J.; Sun, Z. New gallium chalcogenides/arsenene van der Waals heterostructures promising for photocatalytic water splitting. *Int. J. Hydrogen Energy* 2018, 43, 15995–16004.
28. Gupta, U.; Rao, C. Hydrogen generation by water splitting using MoS₂ and other transition metal dichalcogenides. *Nano Energy* 2017, 41, 49–65.
29. Rahman, A.; Jennings, J.R.; Tan, A.L.; Khan, M.M. Molybdenum Disulfide-Based Nanomaterials for Visible-Light-Induced Photocatalysis. *ACS Omega* 2022, 7, 22089–22110.
30. Li, M.; Cui, Z.; Li, E. Silver-modified MoS₂ nanosheets as a high-efficiency visible-light photocatalyst for water splitting. *Ceram. Int.* 2019, 45, 14449–14456.
31. Tang, Y.; Li, X.; Zhang, D.; Pu, X.; Ge, B.; Huang, Y. Noble metal-free ternary MoS₂/Zn_{0.5}Cd_{0.5}S/g-C₃N₄ heterojunction composite for highly efficient photocatalytic H₂ production. *Mater. Res. Bull.* 2018, 110, 214–222.
32. Yuan, Y.-J.; Chen, D.; Zhong, J.; Yang, L.-X.; Wang, J.; Liu, M.-J.; Tu, W.-G.; Yu, Z.-T.; Zou, Z.-G. Interface engineering of a noble-metal-free 2D–2D MoS₂/Cu-ZnIn₂S₄ photocatalyst for enhanced photocatalytic H₂ production. *J. Mater. Chem. A* 2017, 5, 15771–15779.
33. Yin, M.; Sun, J.; Li, Y.; Ye, Y.; Liang, K.; Fan, Y.; Li, Z. Efficient photocatalytic hydrogen evolution over MoS₂/activated carbon composite sensitized by Erythrosin B under LED light irradiation. *Catal. Commun.* 2020, 142, 106029.
34. Hassan, M.A.; Kim, M.-W.; Johar, M.A.; Waseem, A.; Kwon, M.-K.; Ryu, S.-W. Transferred monolayer MoS₂ onto GaN for heterostructure photoanode: Toward stable and efficient photoelectrochemical water splitting. *Sci. Rep.* 2019, 9, 20141.
35. Zhao, G.; Wang, X.; Wang, S.; Rui, K.; Chen, Y.; Yu, H.; Ma, J.; Dou, S.X.; Sun, W. Heteroatom-doped MoSe₂ Nanosheets with Enhanced Hydrogen Evolution Kinetics for Alkaline Water Splitting. *Chem. Asian J.* 2018, 14, 301–306.
36. Li, X.; Zuo, X.; Jiang, X.; Li, D.; Cui, B.; Liu, D. Enhanced photocatalysis for water splitting in layered tin chalcogenides with high carrier mobility. *Phys. Chem. Chem. Phys.* 2019, 21, 7559–7566.
37. Lei, W.; Wang, F.; Pan, X.; Ye, Z.; Lu, B. Z-scheme MoO₃-2D SnS nanosheets heterojunction assisted g-C₃N₄ composite for enhanced photocatalytic hydrogen evolutions. *Int. J. Hydrogen Energy* 2022, 47, 10877–10890.
38. Liu, Y.; Zhou, Y.; Zhou, X.; Jin, X.; Li, B.; Liu, J.; Chen, G. Cu doped SnS₂ nanostructure induced sulfur vacancy towards boosted photocatalytic hydrogen evolution. *Chem. Eng. J.* 2020, 407, 127180.
39. Geng, Y.; Zou, X.; Lu, Y.; Wang, L. Fabrication of the SnS₂/ZnIn₂S₄ heterojunction for highly efficient visible light photocatalytic H₂ evolution. *Int. J. Hydrogen Energy* 2022, 47, 11520–11527.
40. Barawi, M.; Flores, E.; Ferrer, I.J.; Ares, J.R.; Sánchez, C. Titanium trisulphide (TiS₃) nanoribbons for easy hydrogen photogeneration under visible light. *J. Mater. Chem. A* 2015, 3, 7959–7965.
41. Flores, E.; Ares, J.; Sánchez, C.; Ferrer, I. Ternary transition titanium-niobium trisulfide as photoanode for assisted water splitting. *Catal. Today* 2018, 321–322, 107–112.
42. Guo, W.; Wu, D. Facile synthesis of VS₄/graphene nanocomposites and their visible-light-driven photocatalytic water splitting activities. *Int. J. Hydrogen Energy* 2014, 39, 16832–16840.
43. Ikeda, S.; Aono, N.; Iwase, A.; Kobayashi, H.; Kudo, A. Cu₃MS₄ (M=V, Nb, Ta) and its Solid Solutions with Sulvanite Structure for Photocatalytic and Photoelectrochemical H₂ Evolution under Visible-Light Irradiation. *ChemSusChem* 2018, 12, 1977–1983.
44. Li, G.; Deng, X.; Chen, P.; Wang, X.; Ma, J.; Liu, F.; Yin, S.-F. Sulphur vacancies-VS₂@C₃N₄ driven by in situ supramolecular self-assembly for synergistic photocatalytic degradation of real wastewater and H₂ production: Vacancies taming interfacial compact heterojunction and carriers transfer. *Chem. Eng. J.* 2022, 433, 134505.

45. Gopalakrishnan, S.; Paulraj, G.; Eswaran, M.K.; Ray, A.; Singh, N.; Jeganathan, K. VS₂ wrapped Si nanowires as core-shell heterostructure photocathode for highly efficient photoelectrochemical water reduction performance. *Chemosphere* 2022, 302, 134708.
46. Zhong, X.; Tang, J.; Wang, J.; Shao, M.; Chai, J.; Wang, S.; Yang, M.; Yang, Y.; Wang, N.; Wang, S.; et al. 3D heterostructured pure and N-Doped Ni₃S₂/VS₂ nanosheets for high efficient overall water splitting. *Electrochim. Acta* 2018, 269, 55–61.
47. Kurnia, F.; Ng, Y.H.; Amal, R.; Valanoor, N.; Hart, J.N. Defect engineering of ZnS thin films for photoelectrochemical water-splitting under visible light. *Sol. Energy Mater. Sol. Cells* 2016, 153, 179–185.
48. Sánchez-Tovar, R.; Fernández-Domene, R.M.; Montañés, M.T.; Sanz-Marco, A.; Garcia-Antón, J. ZnO/ZnS heterostructures for hydrogen production by photoelectrochemical water splitting. *RSC Adv.* 2016, 6, 30425–30435.
49. Zhang, X.; Zhou, Y.-Z.; Wu, D.-Y.; Liu, X.-H.; Zhang, R.; Liu, H.; Dong, C.-K.; Yang, J.; Kulinich, S.A.; Du, X.-W. ZnO nanosheets with atomically thin ZnS overlayers for photocatalytic water splitting. *J. Mater. Chem. A* 2018, 6, 9057–9063.
50. Arai, T.; Senda, S.-I.; Sato, Y.; Takahashi, H.; Shinoda, K.; Jeyadevan, B.; Tohji, K. Cu-Doped ZnS Hollow Particle with High Activity for Hydrogen Generation from Alkaline Sulfide Solution under Visible Light. *Chem. Mater.* 2008, 20, 1997–2000.
51. Lee, G.-J.; Anandan, S.; Masten, S.J.; Wu, J.J. Photocatalytic hydrogen evolution from water splitting using Cu doped ZnS microspheres under visible light irradiation. *Renew. Energy* 2016, 89, 18–26.

Retrieved from <https://encyclopedia.pub/entry/history/show/77343>